

XMM-Newton Observations of Radio Pulsars B0834+06 and B0826-34 and Implications for Pulsar Inner Accelerator

J. Gil¹, F. Haberl², G. Melikidze^{1,3}, U. Geppert⁴, B. Zhang⁵ and G. Melikidze Jr.¹

ABSTRACT

We report the X-ray observations of two radio pulsars with drifting subpulses: B0834+06 and B0826-34 using XMM-Newton. PSR B0834+06 was detected with a total of 70 counts from the three EPIC instruments over 50 ks exposure time. Its spectrum was best described as that of a blackbody (BB) with temperature $T_s = (2.0^{+2.0}_{-0.9}) \times 10^6$ K and bolometric luminosity of $L_b = (8.6^{+14.2}_{-4.4}) \times 10^{28}$ erg s⁻¹. As it is typical in pulsars with BB thermal components in their X-ray spectra, the hot spot surface area is much smaller than that of the canonical polar cap, implying a non-dipolar surface magnetic field much stronger than the dipolar component derived from the pulsar spin-down (in this case about 50 times smaller and stronger, respectively). The second pulsar PSR B0826-34 was not detected over 50 ks exposure time, giving an upper limit for the bolometric luminosity $L_b \leq 1.4 \times 10^{29}$ erg s⁻¹. We use these data as well as the radio emission data concerned with drifting subpulses to test the Partially Screened Gap (PSG) model of the inner accelerator in pulsars. This model predicts a simple and very intuitive relationship between the polar cap thermal X-ray luminosity (L_b) and the “carousel” period (P_4) for drifting subpulses detected in the radio band. The PSG model has been previously successfully confronted with four radio pulsars whose L_b and P_4 were both measured: PSR B0943+10, PSR B1133+16, PSR B0656+14, and PSR B0628-28. The XMM-Newton X-ray data of PSR B0834+16 reported here are also in agreement with the model prediction, and the upper limit derived from the PSR B0826-34 observation does not contradict with such a prediction. We also include two other pulsars PSR B1929+10 and B1055-52 whose L_b and/or P_4 data became available just recently. These pulsars also follow the prediction of the PSG model. The clear prediction of the PSG model is now supported by all pulsars whose L_b and P_4 are measured and/or estimated.

Subject headings: pulsars: individual (B0834+06, B0826-34)–stars: neutron – X-rays: stars – radiation mechanisms: thermal

1. Introduction

More than forty years after the discovery of radio pulsars, the mechanism by which they emit coherent radio beams is still not fully understood. Also, many properties of this radiation remain a mystery, especially the phenomenon of drifting subpulses. This puzzling phenomenon was widely regarded as a powerful tool for

¹J. Kepler Institute of Astronomy, University of Zielona Góra, Poland

²Max Planck Institute for Extraterrestrial Physics, Garching, Germany

³E. Kharadze Georgian National Astrophysical Observatory, Tbilisi, Georgia

⁴German Aerospace Center, Institute for Space Systems, Berlin, Germany

⁵Department of Physics, University of Nevada, Las Vegas, USA

the investigation of the pulsar radiation mechanism. Recently, this phenomenon received renewed attention, mostly owing to the newly developed techniques for the analysis of the pulsar radio emission fluctuations (Edwards & Stappers 2002,2003; ES02,ES03 henceforth). Using these techniques, Weltevrede et al. (2006 a,b; W06a,b henceforth) presented results of the systematic, unbiased search for the drifting subpulses and/or phase stationary intensity modulations in single pulses of a large sample of pulsars. They found that the fraction of pulsars showing evidence of drifting subpulses is at least 60 % and concluded that the conditions for the drifting mechanism to work cannot be very different from the emission mechanism of radio pulsars.

It is therefore likely that the drifting subpulse phenomenon originates from the so-called inner acceleration region right above the polar cap, which powers the pulsar radiation. In the classical model of Ruderman & Sutherland (1975; RS75 henceforth) the subpulse-associated spark filaments of plasma circulate in the pure Vacuum Gap (VG hereafter) around the magnetic axis due to well known drift of plasma with non-corotational charge density (see Appendix A for more details). There are few periodicities characteristic for this model, called also the pulsar carousel model: the primary period P_3 which can be measured as a distance between the observed subpulse drift bands, the secondary period (apparent when drifting is aliased; Gil & Sendyk 2003 for detailed description), and the tertiary period P_4 (called also the carousel time¹, as it is the time interval after which the gap plasma completes one full circulation around the magnetic pole). The carousel model is widely regarded as a natural and qualitative explanation of the drifting subpulse phenomenon. However, its original version published by Ruderman & Sutherland (1975; RS75 hereafter) predicts too high a drifting rate of the sparks around the polar cap, as compared with the observations of drifting subpulses (e.g. Deshpande & Rankin 1999, 2001; DR99,DR01 henceforth), and too high a heating rate of the polar cap (PC henceforth) surface due to the spark-associated back-flow bombardment, as compared with X-ray observations (e.g. Zhang et al. 2000). Another difficulty of the RS75 model is that recent calculations strongly suggest that the surface binding energy of both ions and electrons are too low to allow the development of a vacuum gap. Indeed, when the surface magnetic field is purely dipolar, then the gap can develop only in magnetars and several highest B-field pulsars (Medin & Lai 2007). Another type of inner accelerator model, named space-charge-limited flow (SCLF, Arons & Scharlemann 1979; Harding & Muslimov 1998), has been discussed in the literature, which assumes that both ions and electrons can be freely striped off the neutron star surface. Although this approximation is valid for most pulsars assuming a pure dipolar field at the polar cap region, a stronger, multipole magnetic field near the polar cap region (which is needed to make a large number of radio pulsars above the radio emission death line, Ruderman & Sutherland 1975; Zhang et al. 2000) would introduce a non-negligible binding energy of ions/electrons (Medin & Lai 2007), which renders the SCLF approximation no longer valid. Another difficulty of the steady-state SCLF model widely discussed in the literature is that it does not predict the existence of any “sparks” that could give rise to the drifting sub-pulses. So, in our opinion, it is not an attractive inner accelerator model to interpret pulsar radio emission.

Motivated by these shortcomings of the otherwise attractive VG model Gil, Melikidze & Geppert (2003; G03 henceforth) developed further the idea of the inner acceleration region above the polar cap by including the partial screening caused by the thermionic flow of ions from the PC surface heated by sparks. We call this kind of the inner acceleration region a “Partially Screened Gap” (PSG hereafter). The PSG is thermally self-regulated in such a way that the surface temperature is always close to but slightly lower (less than 1 percent) than the critical temperature at which the maximum co-rotational ion outflow occurs and the gap is fully screened (see Appendix and/or G03 for more details). Moreover, if the surface temperature

¹designated as \hat{P}_3 in RS75. Although this symbol is still in use, we advocate to replace it by P_4 .

was even few percent lower than the critical temperature, there would be a pure vacuum gap, with all the problems discussed above. Since the actual potential drop in the PSG is much lower than that of the pure VG model (RS75), the intrinsic drift rate and PC heating rate are compatible with measurements of P_4 and L_b , respectively.

The PSG model can be tested if two observational quantities are known: (i) the circulatory period P_4 for drifting subpulses observed in radio-emission and (ii) the X-ray bolometric luminosity L_b of thermal BB radiation from the hot polar cap (see Appendix A). Radio pulsars were targeted since beginning of X-ray astronomy for various scientific reasons. Zhang, Sanwal & Pavlov (2005; Z05 henceforth) were the first who made an attempt to resolve the mystery of drifting subpulses in radio pulsars by observing them in X-rays. They proposed to detect thermal X-ray photons from the PC heated by sparks of plasma likely to be associated with drifting subpulses observed in radio band. Their choice was the best studied drifting subpulse pulsar B0943+10. Using XMM-Newton X-ray observatory they detected a weak source coincident with the target pulsar. Due to very small number of counts detected, no unambiguous spectrum could be obtained. However, they were able to fit the BB model to the data, although a power law model was acceptable as well. Within a BB model they inferred a bolometric luminosity $L_b \sim 5 \times 10^{28}$ erg/s emitted from the hot spot (few MK) with a surface area much smaller (about 60 times) than the conventional polar cap area as defined by the bundle of last closed dipolar field lines. This radio pulsar was well studied by DR99, who described the number of sparks and the circulation time $P_4 = 37.4P$ needed for them to complete one full revolution around the pole (where P is the basic pulsar period). These properties as well could not be accounted for by the conventional theory, and some radical modification of RS75 model was required. It appears that PSG model not only resolves all the problems of the RS75 model, but also offers a clean prediction that can be used to test theories of the inner pulsar accelerator.

2. Previous work

Gil, Melikidze & Zhang (2006b; Paper I henceforth) reanalyzed the B0943+10 case within the PSG model. They derived a very useful formula directly connecting the drifting rate of plasma sparks (measured by the circulation period P_4) and the polar cap heating rate by the back-flow spark bombardment (measured by the bolometric thermal luminosity L_b). By assuming that both the measured quantities are determined by the same value of electric field in the PSG, they obtained a simple formula relating the so-called efficiency of thermal radiation from the hot polar cap with the circulation time

$$\frac{L_b}{\dot{E}} = 0.63 \left(\frac{P_4}{P} \right)^{-2}, \quad (1)$$

where \dot{E} is the pulsar spin-down (see eq. [A3] with $I_{45} = \alpha = 1$ in Appendix A). PSR B0943+10 with its data specified in Table 1, fitted this observational curve quite well (Fig. 1). When one observable parameter in equation (1) is known (L_b or P_4), the other one can be predicted without any free parameters. In Paper I we included B1133+16, the twin pulsar to B0943+10 (at least in the sense of the kinematical properties; see Table 1). In this second case we speculated that the long periodicity of about $30P$ revealed by a number of authors (e.g. W06a,b), is actually the circulatory period $P_4 \sim 30P$. This claim was recently confirmed by sophisticated data analysis of Herfindal & Rankin (2007; HR07 henceforth), although these authors admitted that they did not believe our prediction of P_4 value before their own analysis. The X-rays from B1133+16 were detected by Kargaltsev, Pavlov and Garmire (2006) using Chandra X-ray observatory, who found that their properties were similar to those of the twin pulsar B0943+10. Because of the small number of counts

detected, obtaining an unique spectrum was not possible, like in the case of PSR B0943+10 (ZSP05) . However, the BB model was acceptable and gave the bolometric luminosity $L_b \sim 3 \times 10^{28}$ erg/s emitted from the hot (few MK) and very small polar cap (again much smaller (about 100 times) than the canonical one). As one can see in Figure 1, with the inferred values of P_4 and L_b the pulsar B1133+16 nicely clusters with its twin pulsar along the critical curve expressed by equation (1). Note that filled circle represents our prediction and asterisk represents the estimate of P_4 by HR07.

Encouraged by the observational confirmation of our prediction of P_4 in B1133+16, we applied the same method to two other pulsars for which the measurements or estimates of thermal bolometric luminosity were available (Gil, Melikidze & Zhang 2007; Paper II henceforth). One of the famous Three Musketeers, PSR B0656+14, in which thermal X-rays from small hot polar cap were clearly detected by De Luca, Caraveo, Mereghetti, et al. (2005; DL05 hereafter), was an obvious choice. The BB thermal luminosity $L_b \sim 5.7 \times 10^{31}$ ergs/s (Table 1) inserted into equation (1), returned the predicted value of $P_4 = 20.6 P$. Amazingly, Weltevrede et al. (2006c; W06c henceforth) reported the long-period fluctuation spectral feature $(20 \pm 1)P$ associated with the quasi-periodic amplitude modulation of erratic and strong radio emission detected from this pulsar. Thus, it was tempting to interpreted this period as the circulation time P_4 . With this value of P_4 and L_b shown above, the pulsar B0656+14 fits the equation (1) quite well (Figure 1). Although the drifting subpulses were not apparent in this case, the erratic radio emission reported by W06c was similar to the so-called Q-mode in PSR B0943+10 (showing clearly drifting subpulses in the organized B-mode). The low frequency feature in the fluctuation spectra, identical to that of the B-mode, was found by Rankin & Suleymanova (2006; see their Fig. 6). Asgekar & Deshpande (2001; AD01 hereafter) also detected this feature in the 35-MHz observations of PSR B0943+10(see their Figs.1 and 2). This simply means that the carousel plasma drift is maintained in both regular drifting and erratic (with no drifting subpulses) pulsar emission modes. This is a property of plasma and magnetic field interaction in the gap rather than the structure of this plasma. However, drifting subpulses can be clearly observed only if the gap plasma has some lateral structure, localized sparking discharges for instance.

For the second of the Three Musketeers, PSR B1055-52, we have just found an evidence of a low frequency feature $f \sim 0.042c/P$ (Biggs 1990; B90 henceforth), which can be interpreted as the carousel periodicity $P_4/P \sim 22$. Using this interpretation, which was very fruitful in several other cases discussed above and below, we examine thermal X-ray radiation from the small hot spot detected in this pulsar and attempt to test our PSG model in section 4.4. The third Musketeer (Geminga) is radio quiet, so although it shows thermal BB X-ray emission from the small hot spot, it is not useful for our analysis.

Another pulsar that we could examine using our method of inferring values of P_4 from intensity modulation spectra was PSR B0628-28. As indicated in Table 1, it was detected in X-rays by Tepedelenlioğlu & Ögelman (2005; TÖ05 henceforth), using Chandra and XMM-Newton observatories. This was an exceptional pulsar (called an overluminous one by Becker et al. 2005) with efficiency much larger than that of typical pulsars (Becker & Trümper 1998). For thermal BB component alone $L_b/\dot{E} \sim 1.9 \times 10^{-2}$ (Table 1). This value inserted to equation (1) gives the predicted value of $P_4 \sim (6 \pm 1)P$. Interestingly, W06c reported for this pulsar a relatively short periodicity of $(7 \pm 1)P$ (Table 1). If this periodicity is interpreted as the circulation time P_4 , then this is pulsar is not exceptional at all. It lies on the theoretical curve (eq. [1]) in Figure 1 at exactly the right place. PSR B0628-28 is just another (fourth) pulsar satisfying the predictions of equation (1), which relates the efficiency of thermal X-ray radiation from a hot polar cap to the circulatory periodicity associated with drifting subpulses observed in radio emission.

In order to expand the sample of pulsars that have both L_b and P_4 measured/estimated, we recently launched an observational campaign using the XMM-Newton Observatory. We targeted at two old pulsars

that had P_4 measurements but had no X-ray observations before, and we report on the results of these observations in this paper. The two pulsars, PSR B0826-34 and PSR B0834+06 were observed during the XMM-Newton Cycles AO-5 and AO-6, respectively. Simultaneous radio monitoring was also performed and we will report on these observations in the separate paper. PSR B0826-34 was not detected and we have derived an upper limit for its thermal luminosity. We clearly detected PSR B0834+06, whose spectrum is best modelled by a BB radiation from a small hot spot. We interpret this as due to PC heating by the back-flow bombardment, and found that the bolometric L_b agrees well with equation (1) predicted by the PSG model. For completeness, in this paper we include yet another pulsar PSR B1929+10, whose bolometric thermal luminosity was recently determined by Misanovic, Pavlov & Garmire (2007). We show that this pulsar also satisfies equation (1) by finding a suitable feature in the modulation spectra data base of W06a,b (see section 3.3 for some details). The number of pulsars satisfying and/or being consistent with equation (1) increased to seven. To the best of our knowledge no single counter-example exists. It is worth emphasizing that only pulsars for which both the bolometric luminosity L_b of thermal X-rays from hot polar cap and circulational periodicity P_4 of drifting subpulses observed in radio band are known, can be used for this analysis. In our sample of 8 available cases, 4 pulsars (B0656+14, B1055–52, B0834+06 and B1929+10; see footnote 8 related to the latter case) and 3 others either show an evidence of hot spot thermal emission (B1133+16 and B0628–28) or at least such component cannot be excluded (B0943+10). The last case (B0826–34) is uncertain as we only have an upper limit for X-ray detection (consistent with PSG model).

3. New X-ray data

We have observed two radio pulsars B0834+06 and B0826+34 known for their prominent subpulse drift with the XMM-Newton observatory (Jansen, Lumb, Altieri et al. 2001). We marked them in red color in Figure 1, to distinguish them from previously analyzed four pulsars (marked in black) in Papers I and II. Yet another pulsar B1929+10 (marked in blue in Figure 1) is discussed in Section 3.3, as its values of L_b and P_4 have become recently available.

3.1. PSR B0834+06

The pulsar PSR B0834+06 was observed with XMM-Newton on 2007 November 17 and 18 for a total of ~ 71.7 ks. The EPIC-MOS (Turner, Abbey, Arnaud et al. 2001) and EPIC-PN (Strüder, Briel, Dennerl et al. 2001) cameras were operated in imaging mode (see Table 2). The observation was scheduled at the end of the satellite revolution and the detector background strongly increased when the satellite entered the radiation belts. To maximize the signal to noise ratio we rejected the period of high background which resulted in net exposure times around 50 ks (Table 2).

For the X-ray analysis we used the XMM-Newton Science Analysis System (SAS) version 7.1.0 together with XSPEC version 11.3.2p for spectral modelling. Standard SAS source detection based on a maximum likelihood technique was simultaneously applied to the X-ray images obtained from the three EPIC instruments and five different energy bands (band B1 0.2–0.5 keV, B2 0.5–1.0 keV, B3 1.0–2.0 keV, B4 2.0–4.5 keV and B5 4.5–12.0 keV). A weak source was found at the position of the pulsar at R.A. = 08 37 05.71 and Dec. = 06 10 15.8 (J2000.0) with a 1σ statistical error of $1.7''$. Nearly 150 X-ray sources were detected in the EPIC images and a comparison with catalogues from other wavelength bands yields many correlations within $\sim 0.5''$ of the X-ray positions. This demonstrates that the systematic uncertainty in the astrometry

is small compared to the statistical error of the source position. The X-ray source position is within $1.3''$ of the radio position of PSR B0834+06, consistent within the errors. The positional agreement and other properties of the X-ray source (see below) make a chance coincidence very unlikely.

The total EPIC count rate (summed for the three instruments in the 0.2–4.5 keV band) obtained from the source detection analysis is $(1.4 \pm 0.3) \times 10^{-3}$ cts s $^{-1}$, insufficient for a detailed spectral analysis. To obtain constraints on the shape of the X-ray spectrum we therefore use hardness ratios (X-ray colours) derived from the count rates in the standard energy bands and compare them with those expected from various model spectra. Because the EPIC-PN detector is more sensitive, in particular at low energies where most of the counts are detected, we use only count rates obtained from EPIC-PN. Hardness ratios are defined as $HR1 = (R2-R1)/(R2+R1)$, $HR2 = (R3-R2)/(R3+R2)$, $HR3 = (R4-R3)/(R4+R3)$ and $HR4 = (R5-R4)/(R5+R4)$ with RN denoting the source count rate in band BN. To compare the measured hardness ratios with those inferred from model spectra, we simulated expected EPIC-PN spectra (using XSPEC and the appropriate detector response files) and derived expected count rates and hardness ratios.

The distance to PSR B0834+06 estimated as 643 pc was derived from its dispersion measure of $DM = 12.86$ pc cm $^{-3}$ (from the online ATNF pulsar catalog)². Assuming a 10% ionization degree of the interstellar matter along the line of sight to PSR B0834+06, this converts to a hydrogen column density of $N_H = 4.0 \times 10^{20}$ cm $^{-2}$. Because of the low statistical quality of the X-ray data we are not able to derive tight constraints on the absorbing column density. Therefore, we limit our investigated model parameter space to N_H values between 1.0×10^{20} cm $^{-2}$ (a lower limit which is reached within a distance of 200 pc; Posselt, Popov, Haberl, et al. 2008) and 8.0×10^{20} cm $^{-2}$ (allowing an uncertainty of a factor of 2 in the assumed ionization degree for the conversion from DM to N_H).

As model spectra we tested power-law (PL hereafter) and blackbody (BB hereafter) emission and a combination of the two. In all model spectra absorption was included, assuming elemental abundances from Wilms, Allen & McCray (2000). For the absorbed power-law model we explored the parameter space for N_H between 1.0×10^{20} cm $^{-2}$ and 8.0×10^{20} cm $^{-2}$ with a step size of 1.0×10^{20} cm $^{-2}$ and for the photon index γ between 1 and 5 in steps of 0.2. Figure 2a shows the hardness ratios HR1 versus HR2 derived at the parameter grid points. The measured hardness ratios HR1 and HR2 are drawn with 1σ (solid lines) and 2σ (dotted lines) error bars. The rectangular boxes around the error bars indicate the corresponding confidence areas, although these are in reality limited by error ellipses which fit inside the boxes. As can be seen, the power-law model spectra can not reproduce the measured hardness ratios within their 1σ errors. Allowing 2σ errors would require a relatively steep power-law with a photon index between 2 and 4 and preferentially high absorption.

The results for a BB model with temperatures varying between $kT_{\min} = 80$ eV and $kT_{\max} = 480$ eV in steps of 20 eV (N_H grid as above) are plotted in Figure 2b. The measured hardness ratios are best reproduced by the model with $N_H = 4 \times 10^{20}$ cm $^{-2}$ and $kT = 170$ eV. The 1σ (2σ) confidence range for the temperature is $kT = 170_{-55}^{+65(+120)}$ eV. We determine bolometric luminosity using the model parameters at the grid points (normalizing the simulated spectra to match the observed count rate in the 0.2–4.5 keV band) which yielded $L_b = 8.6_{-2.0}^{+7.6(+14.2)} \times 10^{28}$ erg s $^{-1}$. It is remarkable that the hydrogen column density derived from the “best-fit” BB model of 4.0×10^{20} cm $^{-2}$ is fully consistent with the DM assuming 10% ionization along the line of sight to PSR B0834+06.

We also investigated a combination of BB and PL (with a photon index of 2.0 as typically seen in the

²<http://www.atnf.csiro.au/research/pulsar/psrcat/>

X-ray spectra of pulsars (e.g. Kargaltsev et al. 2006), both subject to the same absorbing column density. As first case the normalization of the power-law component was set to have a flux (for the 0.2–10.0 keV band) in the PL component of 50% of that in the BB component, i.e. a flux ratio of $F_{\text{bb}}:F_{\text{pl}} = 1:0.5$. The hardness ratios are shown in Figure 2c. As expected, HR2, which is most sensitive to the shape of the intrinsic spectral shape, increases with respect to the case of the pure BB due to the contribution of the harder PL component. The 1σ (2σ) confidence ranges are $kT = 140^{+85(+190)}_{-35(-50)}$ eV and $L_b = 9.9^{+4.3(+8.6)}_{-4.4(-4.4)} \times 10^{28}$ erg s $^{-1}$. It should be noted here, that the luminosity of the BB component increases, although a power-law component is added to the model spectrum. This is because the power-law rises toward the low energies and a higher N_{H} values is required to compensate for that. A higher N_{H} in turn increases the bolometric luminosity of the BB component in order to match the observed spectrum (hardness ratios and count rates) again. These effects are also evident in the second case, where we used a flux ratio of $F_{\text{bb}}:F_{\text{pl}} = 1:1$ (Fig. 2d): HR2 increases further and the upper limits for L_b also rise somewhat ($kT = 140^{+80(+210)}_{-40(-55)}$ eV; $L_b = 9.9^{+5.4(+10.9)}_{-4.4(-4.4)} \times 10^{28}$ erg s $^{-1}$).

The above results are summarized in Figure 3 which presents L_b versus kT obtained from the modelled hardness ratios in Figures 2b-2d, where symbols (circle and square for 1σ and 2σ levels, respectively), their colors (red, blue and green for BB, BB(2/3)+PL(1/3) and BB+PL model, respectively) and related numbers, correspond to those used in Figures 2b-2d. We can summarize that thermal radiation from the hot polar cap of PSR B0834+06 is described by $kT = (170^{+180}_{-90})$ eV (or surface temperature of the polar cap $T_s = (2.0^{+2.0}_{-0.9}) \times 10^6$ K and $L_b = (8.6^{+14.2}_{-4.4}) \times 10^{28}$ erg s $^{-1}$, where the 2σ errors are determined by both statistical and model uncertainties.

3.2. PSR B0826-34

The pulsar PSR B0826-34 was observed with XMM-Newton on 2006 November 13 and 14 with the EPIC-MOS and EPIC-PN cameras operated in imaging mode (Table 2). Also during this observation, strong background flaring activity occurred near the end of the observation. After background screening a total exposure time of ~ 38.8 ks was obtained.

We selected this source because it was one of the few pulsars with known P_4 value (Gupta, Gil, Kijak et al. 2004; G04 hereafter). When applying for the XMM-Newton observing time we realized that PSR B0826-34 would be at most a very weak source like PSR B0943+10 (or even weaker) detected by Z05. Indeed the spin-down value was quite low and even our equation (1) predicted the source luminosity twice lower than that of B0943+10. However, B0826-34 is closer to the Earth than B0943+10 by the factor of 1.5. Despite relatively large $\text{DM}=52.9$ pc cm $^{-3}$ we optimistically assumed that the hydrogen column density N_{H} will be similar to that of PSR B0943+10 (with $\text{DM}=15.4$ pc cm $^{-3}$). We speculated that the factor of 3.5 in DM values would be compensated to some degree by the factor of 0.67 in a distance. We did not detect the pulsar, which probably means that the actual value of N_{H} is much higher than assumed, due to some dense cloud of hydrogen along the line of sight to B0826-34. Therefore, we determined the upper limit for thermal X-ray radiation from hot PC from this pulsar.

Because of the higher sensitivity of the EPIC-PN camera we used images from this instrument only. We created images in the energy bands 0.2 – 0.5 keV, 0.5 – 1.0 keV and 1.0 – 2.0 keV and determined 2σ upper limit count rates for the expected source position for each energy band. The total 0.2 – 2.0 keV upper limit was obtained as 2.3 cts s $^{-1}$. Assuming the BB model with $kT = 267$ eV and the absorption column density of 3×10^{20} cm $^{-2}$ (1.4×10^{21} cm $^{-2}$), this converts into an upper limit for the bolometric luminosity of $L_b =$

$1.0 \times 10^{29} \text{ erg s}^{-1}$ ($L_b = 1.45 \times 10^{29} \text{ erg s}^{-1}$). The latter value was conservatively used in Figure 1 (Table 1).

4. Data analysis and model verification

Table 1 and Figure 1 present the observational data of a number of quantities for seven pulsars, in which both P_4 and L_b are known or at least constrained. These data are confronted with the model curve representing equation (1), which is marked by the solid line, accompanied by broken lines describing theoretical errors due to uncertainty with determination of the neutron star moment of inertia (see Appendix A). Two pulsars: B0943+10 and B1133+16 have already been discussed in Paper I, and two others B0656+14 and B0629–28 in Paper II. As argued in Papers I and II these pulsars strongly support our theory (they are presented as black dots in our Figure 1). In the following we study and discuss the results from the remaining three pulsars: B0834+06, B0826–34 (red dots) and B1929+10 (blue dot).

4.1. PSR B0834+06

As already mentioned, the circulatory (tertiary) period P_4 is known for a handful of pulsars, and B0834+06 is one of them. The first measurement of tertiary periodicity for this pulsar was made by Asgekar & Deshpande (2005; AD05 henceforth), who argued that $P_4/P = 15 \pm 0.8$ and the number of circulating sub-beams (sparks) $N = P_4/P_3 = 8$, implying the aliased subpulse drifting with primary period $P_3/P = 1.88 \pm 0.01$. They found a strong low frequency feature in the intensity fluctuation spectrum at $0.07 c/P$ in one sequence of 64 single pulses, supported by side tones flanking the primary feature of $0.46 c/P$ by $\pm 0.066 c/P$. These results seemed quite robust, although a small derived number of sparks (8) as compared with other cases was a bit worrying. We used $P_4/P = 15$ in the scientific justification for XMM-Newton proposal, predicting from equation (1) a quite luminous hot PC in PSR B0834+06, emitting with $L_b = 36 \times 10^{28} \text{ erg s}^{-1}$. The model simulations indicated the count rate of about 0.018 cts s^{-1} , implying a very promising case. Slightly before the scheduled XMM observing session a new estimate was obtained by Rankin & Wright (2007; RW07 henceforth), who argued, using their new Arecibo data and new technique involving a distribution of null pulses, that $P_4/P \sim 30.25$. They argued that the number of sparks and/or subbeams involved in the non-aliased subpulse drift with the true primary period $P_3/P = 2.16 \pm 0.01$ is 14 and thus $P_4/P = 30.24 \pm 0.15$ (Table 1). According to equation (1) this would imply the luminosity 4.16 times lower than $L_b = 36 \times 10^{28} \text{ erg s}^{-1}$ given in our proposal, that is $L_b = 8.85 \times 10^{28} \text{ erg s}^{-1}$ or $L_b/\dot{E} = 0.67 \times 10^{-3}$. Amazingly, this is almost exactly the central value of our best fit for hot BB component in PSR B0834+06 (see Table 1 and Figs. 1 and 3). Thus our measurements interpreted within the PSG model (eq. [1]) strongly support the value of $P_4/P = 30.25 \pm 0.25$ obtained by RW07, while $P_4/P = 15 \pm 0.8$ obtained by AD05 is highly unlikely.

4.2. PSR B0826–34

The carousel rotation time in this pulsar was obtained by means of computer simulations compared with real single pulse data by Gupta, Gil, Kijak et al. 1984. According to equation (1) its value $P_4 = (14 \pm 1)P$ implies the efficiency $L_b/\dot{E} = 3.2 \times 10^{-3}$. These values are marked by the red horizontal error bar labelled by B0826-34. The upper limit 22×10^{-3} is marked as the short arrow above. This pulsar would have to be much more efficient in converting the spin-down power into X-rays to be detected in a 50 ksec XMM-Newton

exposure, or at least a six times longer exposure time would be required.

4.3. PSR B1929+10

Recently Misanovic, Pavlov and Garmire (2007; M07 hereafter) argued that X-rays from PSR B1929+10 include both magnetospheric and thermal components. The BB fit to the latter gives a temperature $kT=0.3$ keV and a projected surface area $A_p \sim 3.4 \times 10^3 \text{ m}^2$ or radius r_b of about 33 meters (much smaller than the canonical $A_{pc} = 2 \times 10^5 \text{ m}^2$ or $r_b \sim 300 \text{ meters}$). This corresponds to the bolometric luminosity $L_b \sim (1-2) \times 10^{30} \text{ ergs s}^{-1}$ emitted from hot ($T = 3.5 \times 10^6 \text{ K}$) polar cap with a radius of about 33 meters. ³ We used the central value of B1929+10 $L_b = 1.17^{+0.13}_{-0.4} \text{ ergs s}^{-1}$ with 2σ errors from M07 (see the top panel in their Figure 11).

For each new pulsar with a known value of thermal bolometric luminosity L_b we search the available data bases for a possible value of P_4 . In case of PSR B1929+10 we found in W06a (their Figure A13) a clear but weak low frequency spectral feature at about $0.02 \text{ c}/P$. This translates into a long periodicity $P_4/P = 50^{+15}_{-5}$, with errors estimated from half-width of the low frequency feature. Going back to Figure 1 we see that the data point (marked in blue color) for B1929+10 (Table 1) fits the theoretical curve very well. This is an important point, as it extends the parameter space to the low efficiency/(long period) region in our Figure 1. The range of parameters for our 7 cases under examination increased to factors of 67 and 7 for the efficiency L_b/\dot{E} and the tertiary period P_4/P , respectively.

4.4. PSR B1055–52

This is a bright radio pulsar showing complex patterns of single pulse intensity modulations. The drifting subpulses are not apparent but this can be the result of a central cut of the line-of-sight (LOS) throughout the emission beam. Indeed, this pulsar has a strong interpulse (IP) separated from the main pulse (MP) by about 145 degrees of longitude (measured between centroids) and both these components have complex profiles, consistent with central LOS traverse. B90 analyzed the fluctuation spectrum and found in part of the profile a small and broad feature at frequency $0.045 \text{ cycles}/P$ with $Q \sim 1.5$. This frequency and low Q can be interpreted as the carousel periodicity $P_4/P = 22^{+11}_{-5}$. Recently, Mitra (2008) confirmed this feature at parts of both MP and IP in his data taken at GMRT (privat information).

The pulsar PSR B1055–52 is a luminous source of X-ray emission. DL05 identified three spectral components in this radiation: Power law magnetospheric emission, cool BB emission from the entire surface of the cooling neutron star, and hot BB emission from a small hot spot. This latter component is of special interest for us and its parameters along with references are listed in Table 1. If the "carousel" hypothesis discussed above is correct, then we expect a correlation between the carousel period P_4 and the bolometric

³Recently, Hui & Becker (2008; henceforth HB07) analyzed the same XMM-Newton data of B1929+19 (using different way of data binning resulting in better photon statistics per spectral bin) and argued that the hot BB component is statistically unjustified. However, if they allowed the BB radius and temperature of the hot spot as the free parameters, then the best fit resulted in very small hot spot area with a radius $r_b = 25.81^{+18.81}_{-25.81} \text{ meters}$, perhaps even smaller than the one obtained by M07. In opinion of HB08 this is unacceptable small as compared with the canonical PC radius. However, within our model this is a result of relatively low dipolar surface magnetic field $B_d = 5 \times 10^{11} \text{ Gauss}$. The actual non-dipolar magnetic field must be much higher (about 400 times) to provide enough binding energy (ML07) for creation of the PSG in this pulsar, which results in the hot spot radius $r_b = 300/20 = 15 \text{ meters}$ (see section 5 for more details).

luminosity L_b from the hot spot, according to our equation (1). As shown in Table 1 and Fig. 1, the bolometric luminosity $L_b = (1.6^{+0.9}_{-0.4})10^{31}$ erg/s, where the errors were estimated from fitting the EPIC-pn spectrum, extracted from the XMM-Newton archival data, with the same model as used by DL05. Although the central values result in the data point lying slightly below the theoretical curve, PSR B1055–52 is certainly consistent with equation (1). Indeed, one can see that values slightly higher than the central one, e.g., $P_4/P \sim 28$ and $L_b/\dot{E} \sim 0.8 \times 10^{-3}$ would result in a very good fit to the equation (1).

5. Conclusions and Discussion

Within the partially screened gap (PSG) model of the inner acceleration region in pulsars developed by G03, we derived in Paper I a simple and clean relationship (eq. [1]) between the thermal X-ray bolometric luminosity L_b from hot PC heated by sparks and the circulation time P_4 of the spark-associated drift detected as the subpulse drift in pulsar radio emission. This relationship expresses the well justified assumption (Appendix A) that both the drifting rate and the polar cap heating rate are determined by the same value of electric field within the inner acceleration region. Indeed, the drifting rate described by measurable P_4 is determined by the tangent (with respect to surface magnetic field) component of the electric field, while the heating rate described by measurable L_b is determined by its component parallel to the surface magnetic field in the (partially screened) gap. In Paper II we showed that PSRs B0943+10, B1133+16, B0628–20 and B0654+14, which were the only pulsars with both L_b and P_4 known at that time, satisfied equation (1) quite well (see also Fig. 1 and Table 1). This suggested that the PSG model may indeed be a reasonable description of the inner accelerator region near the polar cap. In this paper we support this view by demonstrating that another two pulsars (B0834+06, B1929+10 and B1055–52) also satisfy the equation (1). Yet another pulsar B0826-34, in which only the upper limit for L_b was obtained, demonstrated a consistency with equation (1) as well.

Only for a handful of pulsars the circulation (carousel) time was measured or constrained so far. Measurement of P_4 by means of modulation spectral analysis requires a strong unevenness in the circulating system, maybe a distinguished group of adjacent sparks or even just a single spark (see also the scenario discussed by Gil & Sendyk, 2003; GS03 hereafter). Moreover, this feature should persist considerably longer than the circulation time. Such favorable conditions do not occur frequently in pulsars and therefore direct or indirect measurements of P_4 are very rare. In principle, in a clean case one should be able to detect the primary feature P_3 , reflecting the phase modulation of regularly drifting subpulses, flanked by two symmetrical features corresponding to slower amplitude modulation associated with carousel circulation as well as direct low frequency feature $1/P_4$ (like in the case of PSR B0943+10; DR01, AD01 and GS03). However, results of Paper II clearly showed that P_4 can be found also in pulsars without regularly drifting subpulses (and/or in erratic drifting modes). This strongly suggested that no matter the degree of the organization of spark plasma filaments at the polar cap, the slow circumferential plasma drift was always performed at about the same rate in a given pulsar. The problem was how to reveal this motion. Two new methods were discussed or at least mentioned in Paper I. The 2-D phase resolved modulation spectral analysis developed by ES02 and ES03 and implemented by W06a, b was the first one. The second method based on examination of the distribution of nulls in the long sequence of single pulses was recently developed by HR07 and Rankin and Wright (2007; RW07 henceforth). In view of the main results obtained in this paper the latter method deserves some more detailed discussion here.

As discussed in section 3.1 there is a controversy about the actual value of P_4 in PSR 0834+06. AD05 reported that the alias-corrected $P_3/P = 1.88 \pm 0.01$ and $P_4/P = 15 \pm 0.8$, implying the number of sparks

$N = P_4/P_3 = 8$. These authors found just one sequence of 64 pulses in which the fluctuation spectrum analysis revealed the low frequency feature at about $1/15=0.067$. On the other hand RW07 found the non-aliased primary drift periodicity $P_3/P = 2.16 \pm 0.011$ and the number of sparks $N = 15$, implying the tertiary long periodicity $P_4/P = 30.24 \pm 0.15$. This longer cycle with $P_4 \sim 30P$ was supported by our measurements of L_b and PSG model expressed by equation (1). RW07 examined an interaction between nulls and emission in PSR B0834+06. They found that null pulses are not randomly distributed and that the most likely periodicity in their appearance is about $30P$. Following the previous discovery of HR07 that null pulses and drifting subpulses in PSR B1133+16 are associated with the same long periodicity (about $33P$) RW07 convincingly argued that short pseudo-nulls (one pulsar period or less) are just a result of irregular distribution of subpulse subbeams/sparks that persist on time scales of at least hundreds of pulsar periods. The short-time pseudo-nulls appear when the line-of-sight cuts through the low-level emission region in the radio beam. Our results on both B1133+16 and B0834+16 strongly support this picture. The interesting question is then why AD05 obtained such a strong feature at $15P$ for a sequence of 64 single pulses from B0834+06. RW07 admitted that they also found in their data some sequences showing $15P$ periodicity, which seemed to be a sub-harmonic of $30P$ cycle. We noticed yet another problem with the result of AD05. In our opinion, these authors have used incorrectly their equations (2) and (3). In fact, as $\Delta\phi$ they used the longitudinal distance between the profile components and in consequence, the azimuthal magnetic angle between the neighboring subbeams was $\Delta\theta = 50$ degs. This ignored the subpulses appearing in the saddle of the profile. We believe that they should use $\Delta\theta \sim 25$ degs, and as a result, the number of sparks would be $N = 360/25 = 14$ instead 8. This is consisted with $P_4 = NP_3 = 14 \cdot 2.16 = 30.24P$ obtained by RW07 and supported by our results presented in this paper. In summary, we strongly believe that the actual value of P_4 in PSR B0834+06 is close to 30 pulsar periods and that $15P$ corresponds to a first harmonic of the basic cycle. Some evidence of low frequency spectral features at both $0.033 c/P$ and $0.066 c/P$ can be seen in Figure A19 of W06. Moreover, it seems that 14 sparks inferred by RW07 are more likely than 8 sparks inferred by AD05.

The essence of the PSG pulsar model is the presence of a strong, nondipolar surface magnetic field B_s , although it does not appear explicitly in equation (1); see Appendix A for details. The strong value of B_s is necessary for providing enough binding (cohesive energy) to prevent the free flow of iron ions from the surface (Medin & Lai 2007; ML07 hereafter), while the small radius of curvature is needed to develop cascading pair production (e.g. Gil & Melikidze 2002). The latter phenomenon is essential for both shorting out the gap potential drop and providing a dense electron-positron plasma in the radio emission region (eg. Melikidze & Gil, 2000 and Gil, Lyubarski & Melikidze, 2004). When the calculations of ML07 are adapted to the PSG model, then one can derive the dependence of the surface magnetic field on the surface temperature $B_s = B_s(T_s = T_i)$; (we will give detailed description of this topic in a separate paper, but see Appendix A for some details). For the condensed Fe surface this relationship is represented by the solid red line in Figure 7 of ML07. We can apply this apparatus to our case of PSR B0834+06, with $L_b = (6.8_{-1.3}^{+1.1}) \times 10^{28} \text{ erg s}^{-1}$, $T_s = (2.0_{-0.9}^{+2.0}) \times 10^6 \text{ K}$, and the associated effective surface area of the hot spot $A_p = 940 \text{ m}^2$. On the other hand, one can read off from Figure 7 in ML07 the range of values $B_s \sim (1_{-0.6}^{+1.3}) \times 10^{14} \text{ G}$ corresponding to $T_s = (2.0_{-0.9}^{+2.0}) \times 10^6 \text{ K}$. Since the dipolar surface magnetic field and polar cap area are $B_d = 3 \times 10^{12} \text{ G}$ and $A_{pc} = 4.85 \times 10^4 \text{ m}^2$, respectively, we can find the effective surface area $A_p = A_{pc}B_s/B_d = (1.5_{-0.9}^{+1.4}) \times 10^3 \text{ m}^2$. This is consistent with our estimate, in which A_p is about 50 smaller than A_{pc} . Theoretically, this results naturally from the flux conservation of the open magnetic field lines. As pointed out in Paper II (see also references therein), the small size of the hot spot relative to the canonical polar cap area is a typical property of hot BB thermal radiation detected in a number of pulsars. An extreme case was published just recently by Pavlov, Kargaltsev, Wong et al. (2008; P08 hereafter), who reported on the Chandra detection of a

very old (170 Myr) and close to the Earth (0.13 kpc and $0.184^{+0.01}_{-0.017}$ kpc, according to ATNF (Manchester, Hobbs, Teoh et al. 2005) and NE2001 (Cordes & Lazio 2003) database, respectively) radio pulsar PSR J0108-1431, with a very weak dipolar surface magnetic field $B_d = 2.52 \times 10^{11}$ G and a low spindown $\dot{E} = 5.8 \times 10^{30}$ erg s^{-1} . During 30 ks exposure they detected 53 counts and found that the spectrum can be described by PL model or BB model equally well. For the latter model they obtained the bolometric luminosity $L_b = 1.3 \times 10^{28} d_{130}^2$ erg s^{-1} , $T_s = 3.2 \times 10^6$ K and $A_p = 50 d_{130}^2$ m², which translates into the hot spot radius as small as 4 meters. This is the smallest hot polar cap ever observed⁸, with the ratio $b = A_{pc}/A_p = 1.77 \times 10^3 / d_{130}^2$, equal to 1770 or 923 (highest ever obtained) for distances 0.13 and 0.18 kpc, respectively. Accordingly, the actual surface magnetic field $B_s = bB_d$ (see Gil & Sendyk 2000 and ML07) is equal to 4.5 or 2.3×10^{14} G for a distance of 0.13 or 0.18 kpc, respectively. Interestingly, the latter value agrees almost exactly with ML07 (red solid line in their Fig. 7), while the former one implies too high a surface temperature exceeding 5 MK. Thus, the extremely small hot polar cap with $T_s = 3.2$ MK results from the fact that the actual surface magnetic field must be about 1000 times stronger than the dipolar component, in order to provide enough cohesive energy to develop PSG in this pulsar. We can therefore say that the case of PSR J0108-1331 supports strongly the PSG pulsar model, the ML07 cohesive energy calculations for the condensed Fe polar cap surface and NE2001 distance to this pulsar (about 0.184 kpc). If one adopts 0.184 kpc as the proper distance to PSR J0108-1331, then the bolometric BB luminosity is $L_b \sim 2.5 \times 10^{28}$ erg s^{-1} and the efficiency $L_b/\dot{E} \sim 4.3 \times 10^{-3}$. With this value the equation (1) predicts the tertiary periodicity $P_4/P \sim 12$. However, the confirmation of this by means of single pulse radio observations of PSR J0108-1431 seems hopeless with present day possibilities, as the pulsar is also extremely weak in radio band (Tauris, Nicastro, Johnston et al. 1994).

Thus, our PSG model seems to account for the physical phenomena at and above the actual pulsar polar cap quite well. Other available inner acceleration models do not match the observations well. The pure vacuum gap model (Ruderman & Sutherland 1975) has $\eta = 1$. Although it also satisfies Eq.(1), it predicts a very high polar cap heating rate, typically $L_b \sim 10^{-1} - 10^{-2} \dot{E}$ (Zhang et al. 2000), and therefore a very small P_4 . The predicted high L_b has been ruled out by the X-ray observations of many old pulsars (ZSP05, TO05, K06 and this paper), and the predicted low P_4 is also inconsistent with the radio observations. On the other hand, as discussed in §1 the steady-state SCLF model does not predict the existence of the “sparks” whose drifts around the polar cap region provide the most natural interpretation of the observed drifting sub-pulse patterns. A modified unsteady SCLF model (which has not been discussed in the literature) may be able to introduce a sparking-like behavior. Based on the similar logic (i.e. the potential drop along the magnetic field line in the gap is equal to the horizontal potential drop across the spark, see Appendix), a similar equation as Eq.(1) can be derived for the SCLF model. However, since this model introduces a very small effective η value ($\eta \sim (2\pi R_*/cP)^{1/2} \ll 1$, Harding & Muslimov 2001), the predicted polar cap heating rate is too low to interpret the observations, typically $L_b \sim 10^{-4} - 10^{-5} \dot{E}$ (Harding & Muslimov 2002). Also the corresponding drifting velocity is too small so that the predicted P_4 is too long as compared with the radio data. The PSG model predicts an intermediate particle inflow rate, and gives the clean prediction (Eq.[1]) which allows L_b to be a moderate value. This is strongly supported by the data.

In order to solve the binding energy problem in the canonical dipolar magnetic field at the neutron star surface, it has been conjectured that drifting subpulse pulsars are bare strange stars (Xu et al. 1999). The simplest model does not allow a hot polar cap because of the high thermal conductivity of the bare strange star surface layer, which is ruled out by the data. Yue et al. (2006) argued that PSR B0943+10 may be a low mass quark star ($\sim 0.02M_\odot$). However, pulsar drifting seems to be the most common behavior of radio pulsars (W06a,b), some of which have well measured mass around $1.4M_\odot$ (Thorsett & Chakrabarty 1999). We regard that the quark star scenario is no longer attractive in view of the latest observations. The cohesive

energy calculations of Fe ion chains in ultra-strong magnetic field by ML07 seem to be strongly supported by the X-ray observations discussed in this paper.

Finally, we would like to address a hypotheses put forward by Becker, Kramer & Jessner et al. (2006) that in old pulsars ($> 10^6$ yrs) the magnetospheric emission dominates over thermal emission, including both cooling radiation and hot polar cap emission component. These authors suggested that the latter radiation component decreases along with the former one, and if so, the hot polar caps in cooling neutron stars could be formed by anisotropic heat flow due to the presence of the magnetic field rather than by particle bombardment. While in young NSs with core temperature $\simeq 10^8$ K the strong crustal magnetic fields may channel the heat toward the polar cap resulting in T_s of a few MK (Perez-Azorin, Miralles & Pons 2006; Geppert, Küker & Page 2006), in pulsars older than 10^6 years this mechanism is much less efficient and the only viable process that can produce such hot and small polar caps is the back-flow particle bombardment. Almost all pulsars presented and examined in this paper are older than 1 Myr (an exception is 110 kyr PSR B0656+14). For instance, PSR B0834+06 is 3 Myr old and its X-ray emission is dominated by hot BB component (an obvious counter-example arguing against Becker’s claim). In PSR B1929+10 (3.1 Myr old) the luminosity of hot BB component is at least comparable with the magnetospheric X-ray radiation (M07). The very old (170 Myr) rotation powered non-recycled pulsar J0108-1431 clearly shows BB radiation from the hot polar cap (P08), probably accompanied by the magnetospheric emission, but no evidence of cooling radiation from the whole surface, as expected for such an old pulsar.

In summary, both the polar cap full cascade (Zhang & Harding 2000) and the downward outer gap cascade (Cheng, Gil & Zhang 1998) that have been proposed to interpret non-thermal X-ray emission from spindown-powered pulsars are expected to be less significant in pulsars from our sample with respect to the young pulsars. The predicted values of X-ray luminosity in these models are typically lower than that of the polar cap heating in the PSG model (Eq.[1]). In view that other available models of the pulsar inner accelerator (pure vacuum gap model and space-charge-limited flow model) either overpredict or underpredict the polar cap heating level, we conclude that the pulsar inner accelerator is likely partially screened due to a self-regulated sub-Goldreich-Julian flow. Also, the pure vacuum gap model predicts too fast a drifting and the space-charge-limited flow model has no natural explanation for the subpulse drift phenomenon at all. We thus strongly believe that thermal radiation associated with a polar cap heating due to partially screened inner accelerator (PSG) is a common component of pulsar X-ray emission regardless of its age, and this component plays especially significant role in the spectra of old pulsars.

Our results are partly based on observations with XMM-Newton, an ESA Science Mission with instruments and contributions directly funded by ESA Member states and the USA (NASA). We acknowledge the support of the NASA NNX07AF07G and NNX08AC67G grants. JG was partially supported by the Polish State Committee for Scientific Research grant N N203 2738 33 and GM was partially supported by the Polish State Committee for Scientific Research grant N N203 1262 33, as well as by the Georgian NSF ST06/4-096 and INTAS 06-1000017-9258 grants. The XMM-Newton project is supported by the Bundesministerium für Wirtschaft und Technologie/Deutsches Zentrum für Luft- und Raumfahrt (BMWi/DLR, FKZ 50 OX 0001) and the Max-Planck Society. We thank Dr. Dipanjan Mitra for stimulating discussions, critical reading of the manuscript and helpful comments.

A. Inner acceleration region in pulsars

The charge depleted inner acceleration region above the polar cap results from the deviation of a local charge density ρ from the co-rotational charge density (Goldreich & Julian 1969) $\rho_{GJ} = -\mathbf{\Omega} \cdot \mathbf{B}_s / 2\pi c \approx B_s / cP$. For isolated neutron stars one might expect the surface to consist mainly of the iron formed at the neutron star's birth (e.g. Lai 2001). Therefore, the charge depletion above the polar cap can result from binding of the positive ^{56}Fe ions (at least partially) in the neutron star surface. If this is really possible (see Medin & Lai 2006, 2007 and Paper II for details), then the positive charges cannot be supplied at the rate that would compensate the inertial outflow through the light cylinder. As a result, a significant part of the unipolar potential drop develops above the polar cap, which can accelerate positrons to relativistic energies and power the pulsar radiation mechanism, while the electrons would bombard the polar cap surface, causing a thermal ejection of ions, which are otherwise more likely bound in the surface in the absence of additional heating. This thermal ejection would cause partial screening of the acceleration potential drop ΔV corresponding to a shielding factor $\eta = 1 - \rho_i / \rho_{GJ}$ (see GMG03 for details), where ρ_i is the charge density of the ejected ions, $\Delta V = \eta(2\pi/cP)B_s h^2$ is the potential drop and h is the height of the acceleration region. The gap potential drop is completely screened when the total charge density $\rho = \rho_i + \rho_+$ reaches the co-rotational value ρ_{GJ} . In terms of binding of ^{56}Fe ions, the screening factor $\eta = 1 - \exp(C_i - \varepsilon_c / kT_s)$, ε_c is the cohesive energy of the condensed iron surface, T_s is the actual surface temperature, $T_i = \varepsilon_c / kC_i$ is the critical temperature above which the iron ions are ejected with the maximum co-rotation limited rate, and $C_i = 30 \pm 3$ (Medin & Lai 2007).

Because of the exponential sensitivity of the accelerating potential drop to the surface temperature, the actual potential drop should be thermostatically regulated. In fact, when the potential drop is large enough to ignite the cascading pair production, the back-flowing relativistic charges will bombard the polar cap surface and heat it at a predictable rate. This heating will induce thermionic emission from the surface, which will, in turn, decrease the potential drop that caused the thermionic emission in the first place. As a result of these two oppositely directed tendencies, the quasi-equilibrium state should be established, in which heating due to electron bombardment is balanced by cooling due to thermal radiation. This should occur at a temperature slightly lower than the critical temperature above which the polar cap surface delivers thermionic flow at the corotational charge density level. This is an essence of the PSG model. For practical reasons it is assumed that $T_s = T_i$, while in reality T_s is few thousands K lower than T_i , with the latter being strongly dependent on the surface magnetic field B_s . This is illustrated by Figure 7 in Medin & Lai (2007), which was prepared for the pure VG model. The PSG model is realized along the red (for Fe) line in this figure, which shows that for a few MK surface temperatures, as suggested by X-ray observations of pulsar hot spots (see Paper II and references therein) the surface magnetic field must be close to 10^{14} G in all pulsars. For most pulsars this is a much stronger field than that inferred from pulsar spindown due to the magnetic dipole radiation. Therefore, the surface magnetic field in neutron stars must be dominated by crust anchored non-dipolar magnetic anomalies. Such strong and curved surface magnetic field is also necessary for development of the cascading pair production via curvature radiation (e.g. RS75, Gil & Melikidze 2002).

Several models proposed for generating pulsar radio emission based on the concept of vacuum gaps need radius of curvature of surface magnetic field much smaller than the stellar radius (see for e.g. Gil, Melikidze, Mitra 2002). A possibility of generating such fields would be from currents in the neutron stars crust (e.g. Urpin, Levshakov & Iakovlev 1986, Geppert, Rheinhardt & Gil 2003). Mitra, Konar, & Bhattacharya (1999) examined the evolution of multipole components generated by currents in the outer crust. They found that mostly low-order multipoles contribute to the required small radii of curvature and that the structure of the surface magnetic field is not expected to change significantly during the radio pulsar lifetime.

The spark plasma inside PSG must slowly drift with respect to the polar cap surface due to non-corotational charge density. This drift will manifest itself by the observed subpulse drifting, provided the spark arrangement is quasi-stable over time scales of hundreds of pulses or so. The deviation of the charge density from the co-rotational value generates an electric field $\Delta\mathbf{E} = \Delta\mathbf{E}_{\parallel} + \Delta\mathbf{E}_{\perp}$ just above the polar cap surface. The parallel component causes acceleration of charged particles, while the perpendicular component participates in the subpulse drift. The tangent electric field at the polar cap boundary, $\Delta E_{\parallel} = 0.5\Delta V/h = \eta(\pi/cP)B_s h$ (see Appendix A in GMG03 for details). Due to the $\Delta\mathbf{E} \times \mathbf{B}_s$ drift the discharge plasma performs a slow circumferential motion around the magnetic axis (see the next paragraph below) with velocity $v_d = c\Delta E_{\perp}/B_s = \eta\pi h/P$. The time interval to make one full revolution around the polar cap boundary is $P_4 \approx 2\pi r_p/v_d$. One then has

$$\frac{P_4}{P} = 2\frac{r_p}{\eta h \alpha}, \quad (\text{A1})$$

where the coefficient $\alpha = \Delta E_{\perp}/\Delta E_{\parallel}$ should be close to unity. If the plasma above the polar cap is fragmented into filaments (sparks), which determine the intensity structure of the instantaneous pulsar radio beam, then in principle, the circulatory periodicity P_4 can be measured/estimated from the pattern of the observed drifting subpulses (Deshpande & Rankin 1999, Gil & Sendyk 2003). In practice, P_4 is measured from the low frequency features in the modulation spectra obtained from good quality single pulse data of pulsars with drifting subpulses. According to RS75, $P_4 = NP_3$, where N is the number of sparks contributing to the drifting subpulse pattern observed in a given pulsar and P_3 is the primary drift periodicity (distance between the observed non-aliased subpulse drift bands).

The circumferential motion around the magnetic axis like in RS75 holds only when the magnetic and the spin axes are almost parallel (almost aligned rotator, in which the line-of-sight trajectory is almost the circumferential tracks of sparks moving around the magnetic axis). Many pulsars with drifting subpulses have indeed a very broad profile characteristic of the almost aligned rotators: e.g. B0826-34, B0818-41. Others, which are not a broad profile pulsars and show regular drifting must have very high impact angle, i.e. grazing the emission beam. In such cases one cannot exclude the almost aligned geometry. In more general (inclined) case, the spark trajectory does not have to be closed on the polar cap, as sparks should rather follow the trajectory of the line-of-sight projected onto the polar cap, being slightly late behind the star's rotation. However, observations of drifting subpulses in some pulsars do not support such a scenario, being consistent with the circumferential motion of the spark-associated sub-beams of subpulse radiation, even if pulsar is not an aligned rotator. Indeed, an orderly drifting subpulses always demonstrate a systematic intensity modulation, either increasing or decreasing towards the pulse profile midpoint. Also, in pulsars with more central cut of the line-of-sight trajectory the subpulse drift is less apparent (or none) but a characteristic phase-stationary modulation of subpulse intensity modulation persist. These properties strongly suggest that sparks move on closed trajectories on the polar cap, although they do not have to be circular, like in axially symmetric RS75 model, to the extent that in some of the detection of circumferential motion with specified value of P_4 periodicity is possible. A good example of such pulsar with central light-of-sight cut is B0834+06 discussed in this paper. There must be then some agency that makes sparks moving across the the line-of-sight projection on closed trajectories around the local magnetic pole instead around the rotational pole, irrespective of the inclination and impact angles.

The quasi-equilibrium condition is $Q_{cool} = Q_{heat}$, where $Q_{cool} = \sigma T_s^4$ is the cooling power surface density by thermal radiation from the polar cap surface and $Q_{heat} = \gamma m_e c^3 n$ is the heating power surface density due to back-flow bombardment, $\gamma = e\Delta V/m_e c^2$ is the Lorentz factor, $n = n_{GJ} - n_i = \eta n_{GJ}$ is the number density of the back-flowing particles that deposit their kinetic energy at the polar cap surface, η is the shielding factor, n_i is the charge number density of the thermionic ions and $n_{GJ} = \rho_{GJ}/e =$

$1.4 \times 10^{11} b \dot{P}_{-15}^{0.5} P^{-0.5} \text{cm}^{-3}$ is the corotational charge number density and \dot{P}_{-15} is the time derivative of the period in 10^{-15} . It is straightforward to obtain an expression for the quasi-equilibrium surface temperature in the form $T_s = (2 \times 10^6 \text{K})(\dot{P}_{-15}/P)^{1/4} \eta^{1/2} b^{1/2} h_3^{1/2}$ (Paper II), where $h_3 = h/10^3 \text{ cm}$, the parameter $b = B_s/B_d = A_{pc}/A_p$ (Gil & Sendyk 2000, Medin & Lai 2007) describes the domination of the local actual surface magnetic field over the canonical dipolar component at the polar cap, and \dot{P}_{-15} is the normalized period derivative. Here $A_{pc} = \pi r_{pc}^2$ and $A_p = \pi r_p^2$ is the canonical (RS75) and actual emitting surface area, with r_{pc} and r_p being the canonical (RS75) and the actual polar cap radius, respectively. Since the typical polar cap temperature is $T_s \sim 10^6 \text{ K}$ (Paper II), the actual value of b must be much larger than unity, as expected for the highly non-dipolar surface magnetic fields.

Using equation (A1) one can derive the formula for thermal X-ray luminosity as

$$L_b = 2.5 \times 10^{31} \alpha^{-2} \left(\frac{\dot{P}_{-15}}{P^3} \right) \left(\frac{P_4}{P} \right)^{-2}, \quad (\text{A2})$$

or in the simpler form representing the radiation efficiency with respect to the spin-down power $\dot{E} = I\Omega\dot{\Omega} = 3.95 I_{45} \times 10^{31} \dot{P}_{-15}/P^3 \text{ erg/s}$, where $I = I_{45} 10^{45} \text{ g cm}^2$ is the neutron star moment of inertia and $I_{45} = 1_{-0.22}^{+1.25}$ (see Papers I and II for details)

$$\frac{L_b}{\dot{E}} = 0.63 \left(\frac{\alpha^{-2}}{I_{45}} \right) \left(\frac{P_4}{P} \right)^{-2}. \quad (\text{A3})$$

This equation is very useful for a direct comparison with the observations, since it contains only the observed quantities (although it is subject to small uncertainty factors related to the unknown moment of inertia I_{45} and the coefficient α . It does not depend on any details of the sparking gap model like non-dipolar surface magnetic field $b = B_s/B_d$, the height h of the acceleration region and the shielding factor η , since they cancel in the derivation procedure, as they suppose to do so. Indeed, this equation reflects the fact that both the subpulse drifting rate (due to $\Delta \mathbf{E} \times \mathbf{B}_s$ plasma drift) and the polar cap heating rate (due to back-flow bombardment) are determined by the same physical quantity, which is the potential drop across the inner acceleration region just above the polar cap. No other agency should be involved. In practical application of equation (A3) we will set $I_{45} = 1$ and $\alpha = 1$. The former is commonly used and the latter means that the values of the accelerating E_{\parallel} and perpendicular E_{\perp} components of electric field in the PSG are almost the same. It is quite a reasonable assumption, all the more that it seems to be supported observationally (Fig. 1).

REFERENCES

- Arons J., Sharlemann E.T. 1979, ApJ, 231, 854
- Asgekar, A., & Deshpande, A.A. 2001, MNRAS, 326, 1249
- Becker, W., Kramer, W., Jessner, A., et al. 2006, ApJ, 645, 1421
- Biggs, J. D., 1990, MNRAS, 246, 341 (B90)
- Cheng, K. S., Gil, J., & Zhang, L. 1998, ApJ, 493, L35
- Cordes, J.M., & Lazio, T.J.W. 2002, astro-ph/0207156

- De Luca, A., Caraveo, P. A., Mereghetti, S., et al. 2005, *ApJ*, 623, 1051 (DL05)
- Deshpande, A.A., & Rankin, J.M. 1999, *ApJ*, 524, 1008 (DR99)
- Deshpande, A.A., & Rankin, J.M. 2001, *MNRAS*, 322, 438
- Edwards, R.T., & Stappers, B.W. 2002, *A&A*, 393, 733 (ES02)
- Edwards, R.T., & Stappers, B.W. 2003, *A&A*, 407, 273 (ES03)
- Geppert, U., Rheinhardt, M., & Gil, J., 2003, *A&A*, 412, L33
- Geppert, U., Küker, M., & Page, D. 2006, *A&A*, 457, 937
- Gil, J., & Melikidze, G. I. 2000, *ApJ*, 544, 1081
- Gil, J., & Sendyk, M., 2000, *ApJ*, 541, 351
- Gil J., & Melikidze, G.I., 2002, *ApJ*, 577, 909
- Gil, J. A., Melikidze, G. I. and Mitra, D., 2002, *aap*, 388, 235G
- Gil J., & Sendyk, M. 2003, *ApJ*, 585, 453
- Gil, J., Melikidze, G.I., & Geppert, U. 2003, *A&A*, 407, 315 (G03)
- Gil J., Lyubarsky, Y., & Melikidze, G.I. 2004, *ApJ*, 600, 872
- Gil J., Melikidze, G., & Zhang, B. 2006a, *ApJ*, 650, 1048
- Gil J., Melikidze G., & Zhang, B. 2006b, *A&A*, 457, 5 (Paper I)
- Gil J., Melikidze G., & Zhang, B. 2007, *MNRAS*, 376, L67 (Paper II)
- Mitra, D., Konar, S., Bhattacharya, D, 1999, *MNRAS*, 307, 459
- Goldreich P., & Julian, H. 1969, *ApJ*, 157, 869
- Gupta, Y., Gil J., Kijak, J., & Sendyk, M. 2004, *A&A*, 426, 229
- Harding, A. K., & Muslimov, A. G. 1998, *ApJ*, 508, 328
- Harding, A. K., & Muslimov, A. G. 2001, *ApJ*, 556, 987
- Harding, A. K., & Muslimov, A. G. 2002, *ApJ*, 568, 862
- Herfindal, J.L., & Rankin, J.M. 2007, *MNRAS*, 380, 430 (HR07)
- Hui, C.Y., & Becker, W. 2008, *astro-ph/07070800* (HB08)
- Jansen, F., Lumb, D., Altieri, B., et al. 2001, *A&A*, 365, L1
- Kargaltsev O., Pavlov G.G., & Garmire, G.P. 2006, *ApJ*, 636, 406 (K06)
- Lai, D. 2001, *Rev. Mod. Phys.*, 73, 629
- Manchester, R.N., Hobbs, G.B., Teoh, A., & Hobbs, M. 2005, *AJ*, 129, 1993

- Misanovic, Z., Pavlov, G.G., & Garmire, G.P. 2007, astro-ph/0711417 (M07)
- Medin Z., & Lai, D. 2007, MNRAS, 382, 1833 (ML07)
- Medin, Z., & Lai, D. 2006, Phys. Rev. A, 74, 062508
- Perez-Azorin, J.F., Miralles, J.A., & Pons, J.A. 2006, A&A, 451, 1009
- Posselt, B., Popov, S. B., Haberl, F., et al. 2008, A&A(in press)
- Rankin, J.M., & Suleymanova, S.A. 2006, A&A, 453, 679
- Rankin, J.M., & Wright, G.A.E. 2007, MNRAS, 379, 507 (RW07)
- Ruderman, M.A., & Sutherland, P.G. 1975, ApJ, 196, 51 (RS75)
- Strüder, L., Briel, U., Dennerl, K., et al. 2001, A&A, 365, L18
- Tauris, T.M., Nicastro L., Johnston, S., et al. 1994, ApJ, 428, L53
- Tepedelenlioglu E., & Ögelman, H. 2005, ApJ, 630, 57 (TÖ05)
- Turner, M. J. L., Abbey, A., Arnaud, M., et al. 2001, A&A, 365, L27
- Thorsett, S. E., & Chakrabarty, D. 1999, ApJ, 512, 288
- Urpin, V. A.; Levshakov, S. A.; Iakovlev, D. G., 1986, MNRAS, 219,703
- Weltevrede, P., Edwards, R.I., & Stappers, B.W. 2006a, A&A, 445, 243 (W06a)
- Weltevrede, P., Wright, G.A.E., Stappers B.W., & Rankin, J. M. 2006b, A&A, 459, 597 (W06b)
- Wilms, J., Allen, A., & McCray, R. 2000, ApJ, 542, 914
- Xu, R. X., Qiao, G. J., & Zhang, B. 1999, ApJ, 522, L109
- Yue, Y. L., Cui, X. H., & Xu, R. X. 2006, ApJ, 649, L95
- Zhang, B., Harding A., & Muslimov A. 2000, ApJ, 531, L135
- Zhang, B., & Harding A.K. 2000, ApJ, 532, 1150
- Zhang, B., Sanwal D., & Pavlov, G.G. 2005, ApJ,624, L109 (Z05)

Table 1. Thermal X-ray radiation for hot polar cap in pulsars with drifting subpulses.

PSR	P (s)	\dot{P}_{-15}	\dot{E} (erg s ⁻¹)	P_4/P	Ref.	L_b (erg s ⁻¹)	Ref.	L_b/\dot{E}	T_s (10 ⁶ K)
B0943+10	1.09	3.49	1.0×10^{32}	$37.4^{+0.4}_{-1.4}$	1	$(5.0^{+0.6}_{-1.7})10^{28}$	8	$(0.49^{+0.06}_{-0.16})10^{-3}$	$3.1^{+0.9}_{-1.1}$
B1113+16	1.19	3.73	8.8×10^{31}	33 ± 3	2				
				32 ± 4	3	$(6.8^{+1.1}_{-1.3})10^{28}$	9	$(0.77^{+0.13}_{-0.15})10^{-3}$	$3.2^{+1.9}_{-1.0}$
B0834+06	1.27	6.8	1.3×10^{32}	30.2 ± 0.2	4	$(8.6^{+14.2}_{-4.4})10^{28}$	5	$(0.67^{+1.1}_{-0.6})10^{-3}$	$2.0^{+2.0}_{-0.9}$
B1929+10	0.23	1.16	3.9×10^{33}	50^{+15}_{-5}	5	$(1.17^{+0.13}_{-0.4})10^{30}$	10	$(0.29^{+0.04}_{-0.09})10^{-3}$	$3.5^{+0.2}_{-0.5}$
B0656+14	0.38	55.0	3.8×10^{34}	20 ± 1	6	$(5.7^{+0.6}_{-0.8})10^{31}$	11	$(1.5 \pm 0.3)10^{-3}$	$1.25^{+0.03}_{-0.03}$
B1055–52	0.19	5.8	3.0×10^{34}	22^{+11}_{-5}	13	$(1.6^{+0.88}_{-0.42})10^{31}$	11	$(0.53^{+0.88}_{-0.42})10^{-3}$	$1.8^{+0.06}_{-0.06}$
B0628–28	1.24	7.12	1.5×10^{32}	7 ± 1	6	$(2.9^{+1.5}_{-0.8})10^{30}$	12	$(1.9^{+1.0}_{-0.5})10^{-2}$	$3.3^{+1.3}_{-0.6}$
B0826–34	1.85	0.99	6.2×10^{30}	14 ± 1	7	$< 1.45 \cdot 10^{29}$	5	$< 22 \cdot 10^{-3}$	

Note. — Errors in L_b and T_s correspond to 2σ (90 % confidence) level. References: 1 - DR99; 2 - Paper I; 3 - HR07; 4 - RW07; 5 - this Paper; 6 - Paper II; 7 - G04; 8 - Z05; 9 - K06; 10 - M07; 11 - DL05; 12 TO05; 13 B90

Table 2. The XMM-Newton EPIC observations of PSR B0826–34 and PSR B0834+06.

Pointing direction R.A. (J2000.0) Dec.		Sat. Rev.	Inst. ^a	Start time (UT)	End time	Exp. ^a ks
PSR B0826–34 (Observation ID 0400020101):						
08 28 16.6	-34 17 07	1269	PN	2006-11-13 13:44:24	2006-11-14 09:19:30	38.83
			M1	13:22:03	09:19:35	–
			M2	13:22:03	09:19:50	–
PSR B0834+06 (Observation ID 0501040101):						
08 37 05.6	06 10 15	1454	PN	2007-11-17 13:44:24	2007-11-18 09:19:30	48.95
			M1	13:22:03	09:19:35	53.30
			M2	13:22:03	09:19:50	54.44

^aThe three EPIC instruments were operated in full frame CCD readout mode with 73 ms frame time for PN and 2.6 s for MOS with thin optical blocking filters.

^bNet exposure times after background screening.

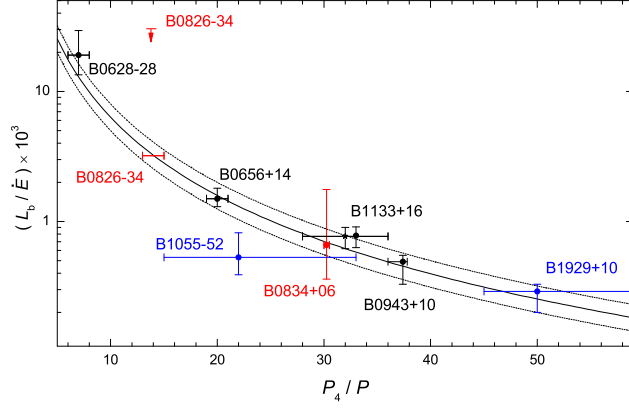


Fig. 1.— The efficiency of thermal X-ray emission from a hot polar cap L_b/\dot{E} versus circulation period P_4 of drifting subpulses in the radio band. The solid curve represents the prediction of the PSG model (eq. [1]), while the dotted curves correspond to uncertainties in determining the moment of inertia (see Appendix A). The values of P_4 and L_b along with their error bars (2σ) and references for the data are given in Table 1.

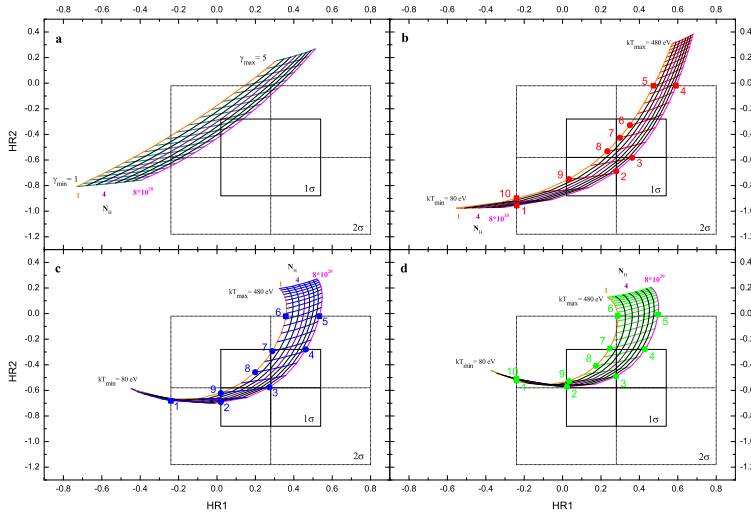


Fig. 2.— **a.** Hardness ratios HR1 and HR2 derived for a grid of power-law model spectra with varying column density N_H and photon index γ compared to the measured values from the EPIC-PN data of PSR B0834+06. The cross and box drawn with full lines indicate 1σ and dotted lines 2σ confidence regions. **b.** As in Figure 2a but for an absorbed blackbody model with kT ranging from 80 to 480 eV, with a step of 20 eV. **c.** As in Figure 2b but for a model with blackbody and power-law component. Both components are absorbed by the same N_H and the relative (0.2–10.0 keV) flux ratio is 1:0.5, respectively. **d.** As in Figure 2c but for a flux ratio of 1:1.

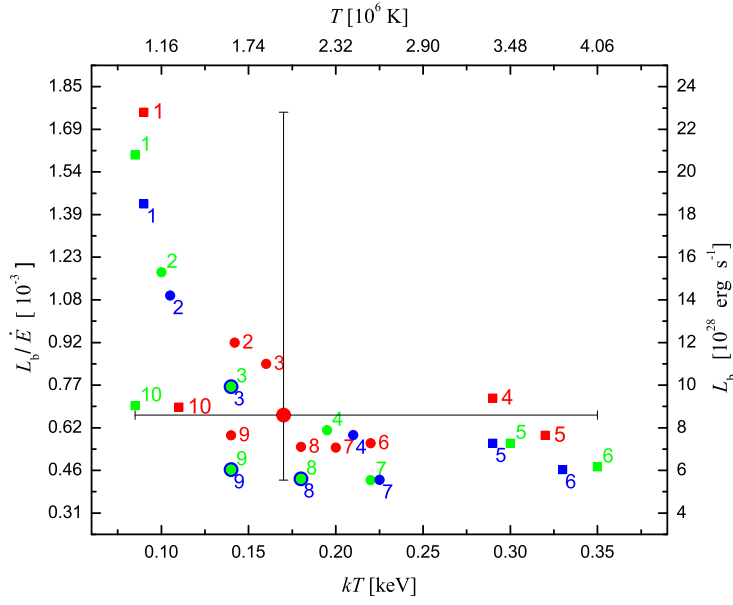


Fig. 3.— Thermal luminosity L_b and its efficiency L_b/\dot{E} versus the polar cap temperature kT for B0834+06 derived by means of XSPEC spectral modelling for color marked and numbered points in Figures 2b-2d. The large red circle corresponds to the best fit of the BB model and the error bars include the model uncertainties.